Int. J. Electrochem. Sci., 7 **(2012)** 9592 - 9608

International Journal of
ELECTROCHEMICAL
SCIENCE
www.electrochemsci.org

Electrochemical Assessment of the Self-Healing Properties of Cerium Doped Sol-Gel Coatings on 304L Stainless Steel Substrates

Roohangiz Zandi Zand[1], *Kim Verbeken*[2], *Annemie Adriaens*[1,*]

[1]Department of Analytical Chemistry, Ghent University, Krijgslaan 281-S12, B-9000, Ghent, Belgium
[2]Department of Materials Science and Engineering, Ghent University, Technologiepark 903, B-9052 Zwijnaarde (Ghent), Belgium
[*]E-mail: annemie.adriaens@ugent.be

Received: 24 July 2012 / *Accepted:* 31 August 2012 / *Published:* 1 October 2012

The present work aims at assessing the corrosion behavior of 304L stainless steel substrates pre-treated with 3-glicidoxypropyltrimethoxy silane (GPTMS) solutions modified with cerium nitrate or cerium oxide nanoparticles. Furthermore, the work aims at evaluating the self-healing properties of the dopant in intact and artificially scratched silane films via natural salt spray tests, electrochemical impedance spectroscopy (EIS) and d.c. potentiodynamic polarization. The morphological features of the coated substrates were evaluated by atomic force microscopy (AFM) and optical microscopy. The results confirmed the formation of transparent cerium modified sol-gel films without any defect and cracks and revealed the formation of a comparatively smooth nanostructure surface with a small heterogeneity in coating thickness in the sol-gel coatings modified with $Ce(NO_3)_3.6H_2O$. Corrosion tests indicated that the CeO_2 nanoparticles have good corrosion inhibition properties on scratched surfaces due to their ability to complex other species, therefore contributing for the stabilization of the passive film. In this way, these particles display an anodic inhibition mechanism. It was found that the positive impact, both in the barrier properties and corrosion inhibition, was significantly improved by modifying the silane solution with cerium nitrate. Presence of cerium nitrate, reinforces the barrier properties of the silane films, reducing the corrosion activity and self-healing the corroded areas.

Keywords: 304L Stainless steel; Corrosion inhibition; Self-healing; Barrier properties; Sol-gel coating.

1. INTRODUCTION

Pre-treatments based on functional silane coatings present prime technological interest as they provide different chemical functionalities on a wide range of substrates either metallic or non-metallic.

The silane coatings are usually uniform, robust and reliable, presenting a lateral resolution in the nanometer regime [1–9]. The good barrier properties of the silane coatings are due to the formation of a dense –Si–O–Si– network, which hinders the penetration of aggressive species towards the metallic substrate. Thus, the effectiveness of the pre-treatments based on silane coatings is strongly dependent on the barrier properties of the film [10-13]. These barrier properties can be enhanced in order to make the silane coatings even more effective. Such goal can be achieved by the addition of small amounts of chemicals possessing specific corrosion inhibition properties, preferentially self-healing properties [14].

Recently, a new research trend in sol–gel processes has been oriented towards the development of sol–gel coatings doped with environmentally friendly inhibitors, such as cerium compounds [14-19]. These systems try to combine the "barrier protection" effect of sol–gel coatings with the "corrosion inhibition" effect of the cerium ions [11, 19]. Corrosion is inhibited by cerium ions that migrate through the coating to the location of the attack (a defect in the coatings) and then react to passivate the site. Thus, cerium ions act as cathodic inhibitors at active sites through precipitation of insoluble cerium hydroxide at local regions of high pH [19,20].

The corrosion inhibition properties of cerium compounds have been widely discussed in literature. Pepe et al. [7,16], for instance, studied the role of incorporating cerium ions in hybrid silica sol-gel coatings prepared with tetraethylorthosilicate [$Si(OC_2H_5)_4$, TEOS] and methyltriethoxysilane [$SiCH_3(OC_2H_5)_3$, MTES] doped with cerium salts on AISI 304 stainless steel and aluminum substrates. Results have shown an improvement of the corrosion protection in NaCl solutions. The explanation for this behavior can be found in the reaction of cerium (III and IV) and chromium (in the case of stainless steel) ions with the hydroxyls groups to the precipitation of cerium and chromium oxide/hydroxide on cathodic areas that can act as a barrier for the subsequent entrance of the oxygen to the reactive sites. Schem et al. [20] studied the electrochemical behavior of aluminum alloy 2024-T3 treated with hybrid sol-gel coating containing cerium oxide nanoparticles. Their studies indicate a general beneficial effect of incorporation of ceria nanoparticles, although the performance of the coated alloy depends on the nanoparticle content. The electrochemical polarisation behavior revealed that the coating decreased the anodic current density by about seven orders of magnitude compared with the uncoated alloy, with high breakdown potentials in chloride-containing solution.

Montemor et al. [21] investigated the role of CeO_2 nanoparticles used as fillers for hybrid silane coatings applied on galvanized steel substrates. Electrochemical impedance (EIS) and scanning vibrating electrode technique (SVET) measurements showed that the modified coatings have improved barrier properties and highlight the corrosion inhibition effect of ceria nanoparticles activated with Ce(III) ions.

In our previous work [22] it was reported that silane coatings modified with cerium nitrate hexahydrate provide very good barrier properties and improve the corrosion protection in comparison to non-modified silane coatings, when applied on 304L stainless steel substrates. The cerium inhibited system shows a slower electrochemical evolution than the non-inhibited one, because the inhibition effect of cerium ions slows down the corrosion kinetics.

Also cerium doped sol–gel coatings can supply self-healing abilities, which can automatically repair the corroded areas, thereby providing long-term corrosion protection. Self–healing can be

defined as the partial recovery of the protective properties of the coated system when damaged [12,21]. The most suitable way to evaluate self-healing ability is via the application of an artificial defect on the surface and monitoring of the electrochemical behavior using electrochemical impedance spectroscopy [12,21]. In this regard, in the present work, the self-healing ability of cerium modified sol-gel coatings on 304L stainless steel substrates was investigated by monitoring the electrochemical behavior of the coated samples before and after defect application. Cerium nitrate and cerium oxide nanoparticles were used as cerium sources and the electrochemical behavior of the sol-gel coatings doped with cerium nitrate was compared with that of sol-gel coatings containing cerium oxide nanoparticles. In this study, the coated samples were immersed in the electrolyte for one week and after this period a defect was created on the surface as described in the experimental section. The corrosion behavior of the sol–gel coatings was investigated using natural salt spray tests, EIS and potentiodynamic polarization. Additionally, the morphological features of the coated substrates were evaluated by atomic force microscopy (AFM) and optical microscopy.

2. EXPERIMENTAL

2.1. Sample preparation

304L stainless steel (17.65 mass. % Cr, 8.59 mass. % Ni, 1.75 mass. % Mn, 0.41 mass. % Si, 0.25 mass. % Mo, 0.017 mass. % C, 0.45 mass. % Cu, 0.032 mass. % P, 0.0050 mass. % S, 0.0049 mass. % Al, Fe balance) was used as substrate. In this study, coupons with an area of 4.98 cm^2 and a thickness of 0.1 cm were used. The coupons were successively ground with 600 and 1200 grit emery paper, degreased with acetone in an ultrasonic bath for 10 min. Chemical etching was performed by dipping the samples into an alkaline solution (1 M NaOH solution) for 5 min at 50 ºC. After rinsing in tap water and then in deionised water, the cleaned substrates were air-dried.

The silane solution was prepared by adding 4.084 mL of 3-glicidoxypropyltrimethoxy silane or GPTMS (Merck) to 0.5 mL of HCl-acidified water (pH = 2) (H_2O/Si mole ratio = 0.5 [23]). The solution was placed in a sealed beaker and stirred at room temperature for 20 min at a rate of 240 rpm to hydrolyse and condensate the silane precursors. $Ce(NO_3)_3.6H_2O$ (Fluka) and CeO_2 nanoparticles (10 wt % in water, particle size < 25 nm, Sigma Aldrich) were used as sources of cerium and were added at the end of this step of synthesis, followed by stirring for 10 min. The Ce/Si mole ratio in both cases was 0.1. In a following step, 2.111 g of bisphenol A (BPA) (Merck) was added to the solutions as a cross-linking agent (BPA/Si mole ratio = 0.5). The latter has shown to have a significant effect on the morphology and corrosion resistance of the coating [22]. BPA was dissolved by mixing the solution for 80 minutes. To accelerate the condensation reaction, 0.0152 mL of 1-methylimidazol (MI) (Merck) (MI/Si mole ratio = 0.01) was added to the solution, followed by stirring for 5 min. The result in both cases ($Ce(NO_3)_3.6H_2O$ and CeO_2 solution) was a clear and colorless homogenous solution. Finally, the cleaned substrates were dipped for 1 min in the silane solutions. The coated specimens were left to dry at room temperature for 24 hours, which was followed by a 25-130 °C curing process for 90 minutes to

initiate extensive cross-linking in the hybrid films [24]. The coating thickness was measured by profilometry (Check line 3000 pro, Germany).

2.2. Analytical methods

2.2.1. Microscopic imaging

Atomic force microscopy (AFM) images were obtained in ambient conditions with a Multimode scanning probe microscope (Digital Instruments – USA) equipped with a Nanoscope IIIa controler. 10 μm scans were recorded in tapping mode with a silicon cantilever (OTESPA – Veeco). Nanoscope software version 4.43r8 was used for surface roughness analysis after the recorded images were modified with an X and Y Plane Fit Auto procedure.

The surface characterization of the coatings before and after corrosion tests, were assessed using an optical microscope Nikon SMZ 800 with operating software NIS Elements D 3.0.

2.2.2. Salt spray testing

The corrosion performance of the coated substrates was evaluated in a neutral salt spray test, following the ASTM B117 procedure [25] and employing a 5 % sodium chloride solution. Prior to exposure, the back and the edges of the plates were covered with adhesive tape. An artificial scratch was made in the coating that penetrated to the substrate to examine possible delamination. Visual assessments of the macroscopic surfaces were carried out at various time intervals during the exposure time.

2.2.3. Electrochemical analysis

To evaluate the corrosion inhibition performance of the modified silane films, a defect in the form of a scratch was made on the surface using a needle. The diameter of the circular defect was around 1 mm. Electrochemical impedance measurements (EIS) and potentiodynamic polarization tests were carried out to monitor the corrosion performance of intact and scratched silane-treated 304L stainless steel substrates in a 3.5 % NaCl solution using an Autolab PG-STAT 20 potentiostat equipped with a frequency response analyzer module. A three-electrode system was used, in which a Ag/AgCl KCl_{sat} electrode, a platinum mesh electrode and the sample were used as reference, counter, and working electrodes, respectively. The EIS measurements were performed at the open circuit potential. The data were obtained as a function of frequency (frequency range of 10^5 Hz to 10^{-2} Hz), using a sine wave of 10 mV amplitude peak to peak. All EIS measurements were carried out at room temperature and the samples were immersed in the electrolyte solution 30 min before the data was acquired and measurements were performed periodically. For each experiment, 4 replicate measurements were done. Impedance fitting was performed using the appropriate equivalent circuits by means of Z-view software (Scribner Associates Inc.).

The potentiodynamic measurements were taken within the range of -1500 to 1000 mV versus Ag/AgCl KCl_{sat} at a rate of 1 mV/s. Also here 4 replicate measurements were performed. The Tafel extrapolation method (conducted according to the ASTM Standard G3-89, 2004) [26] was utilized for determining I_{corr} and E_{corr}.

3. RESULTS AND DISCUSSION

3.1. Atomic force microscopy studies

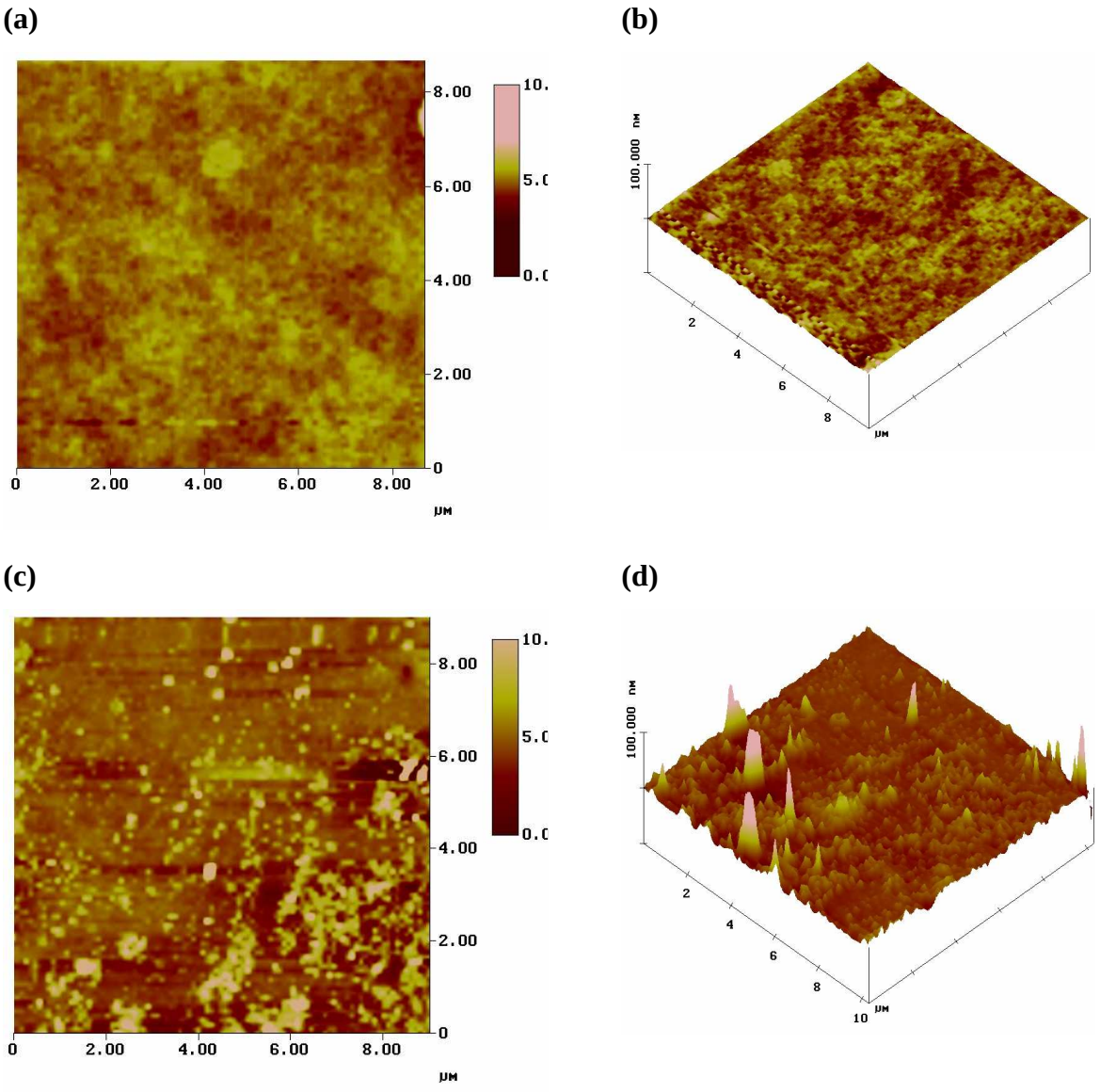

Figure 1. AFM (a, c) top view and (b, d) topographic images taken on the 304L stainless steel specimens coated with the sol-gel coatings modified with $Ce(NO_3)_3.6H_2O$ (a, b) and CeO_2 nanoparticles (c, d).

Figure 1 present AFM (a, c) top view and (b, d) topographic images recorded on the 304L stainless steel specimens covered with the sol-gel coatings modified with $Ce(NO_3)_3.6H_2O$ and CeO_2 nanoparticles respectively.

The AFM images of the sol-gel coating modified with $Ce(NO_3)_3.6H_2O$ (Figures 1a and b) reveal a comparatively smooth nanostructure surface with RMS (root mean square) surface roughness of 0.227 nm. Interestingly, the rather low color contrast in figure 1a suggests a limited heterogeneity of the coating thickness. In addition, no agglomerates are present on the surface.

In case of the sol-gel coating modified with CeO_2 nanoparticles (Figures 1c and d), the nanosized particles incorporated into the film matrix are clearly defined in these scans. The distribution of the nanoparticles is relatively uniform and the RMS roughness is 2.145 nm. Several particles in the hybrid matrix show a larger diameter and seem to result from agglomerates of smaller ones.

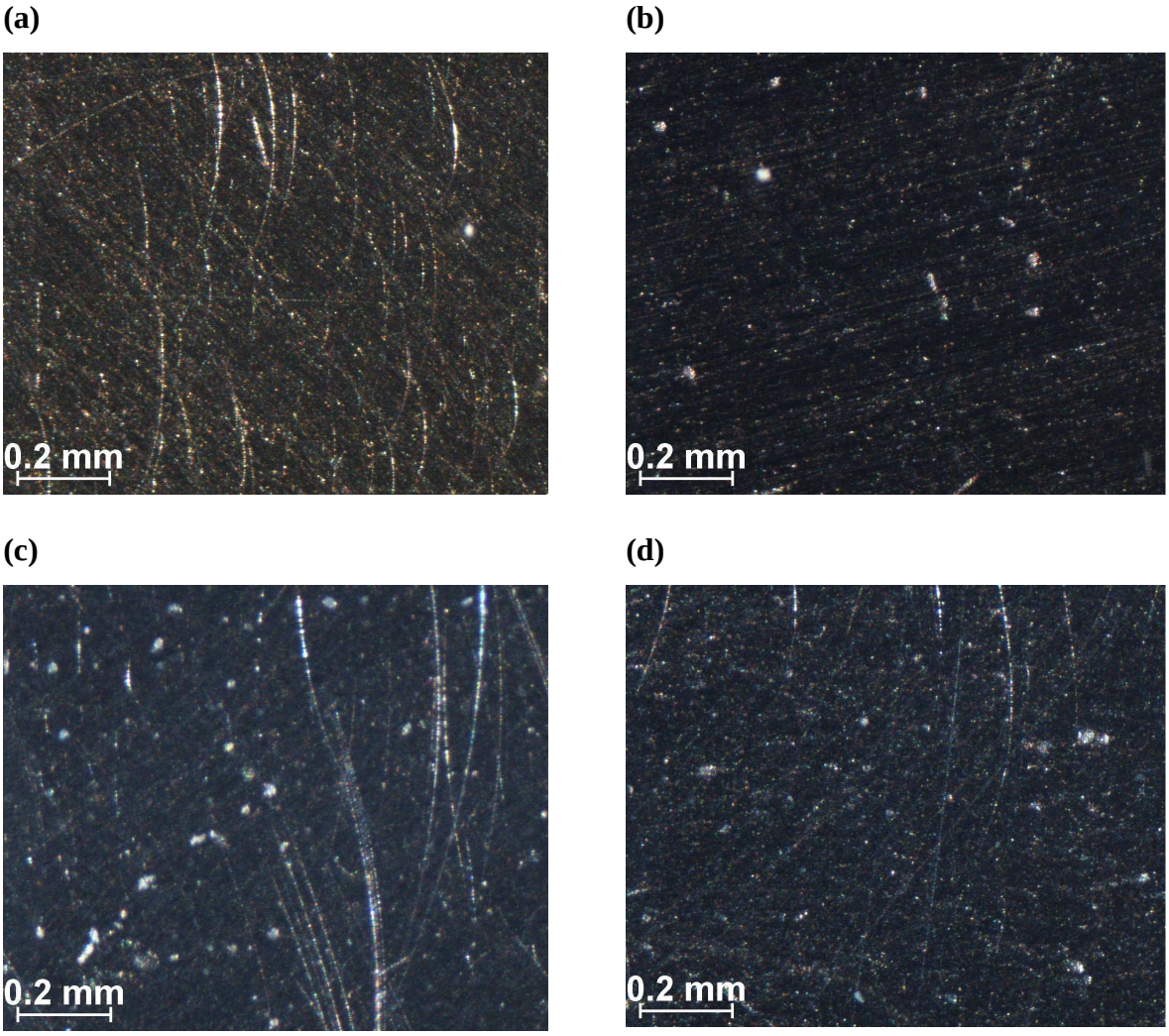

Figure 2. Optical photographs of the 304L stainless steel specimens coated with the sol-gel coatings modified with $Ce(NO_3)_3.6H_2O$ (a, b) and CeO_2 nanoparticles (c, d) before (a, c) and after 20 days of immersion (b, d) in 3.5% NaCl solution.

Furthermore, there is a sharper color contrast in the top view image suggesting stronger height differences. Interestingly, the color contrast is uniformly distributed throughout the image, again suggesting heterogeneity of the coating thickness.

3.2. Surface characterization before and after corrosion

Optical photographs of the sol-gel coated steel specimens before and after 14 days of immersion in 3.5 % NaCl solution (before and after the application of the defect) are presented in figure 2. All the coatings appear crack-free and transparent in such a way that the polishing marks on the underlying metal substrates are visible through the coatings. The photograph of the sol-gel coating modified with $Ce(NO_3)_3.6H_2O$ before corrosion reveals a smooth surface morphology (Figure 2a), but after the corrosion test, the surface of the coating is found to contain a few heterogeneities (Figure 2b) which can be micropores or defects in the coating. Photographs of the sol-gel coating modified with CeO_2 nanoparticles before and after the corrosion test reveal a less homogenous coating with the presence of several heterogeneities (Figures 2 c and d). These heterogeneities are probably due to the presence of agglomerates of nanoparticles, micropores or defects in the coating.

3.3. Performance in the salt spray test

The traditional salt spray coating corrosion resistance evaluation technique was used to evaluate the corrosion performance of the sol–gel films. Figure 3 shows the photographs of the coated 304L stainless steel surfaces coated with $Ce(NO_3)_3.6H_2O$ and CeO_2 nanoparticles modified sol-gel coatings after 2000 hours of salt spray exposure. For the substrate coated with $Ce(NO_3)_3.6H_2O$ modified sol-gel coating (average thickness of the coating= 60.6 ± 11.96 µm) (Figure 3a), no signs of blistering, delaminating and corrosion exhibited and the sample still retains its originally shiny surfaces. In contrast, for the substrate coated with the CeO_2 nanoparticles modified sol-gel coating (average thickness of the coating= 60.66 ± 13.51 µm) (Figure 3b), small blistering around the scratched area exhibited that marked by circles in the figure. Therefore, these data confirm the good corrosion protection for a long term, of the silane sol–gel coatings modified with $Ce(NO_3)_3.6H_2O$.

3.4. EIS results

Figure 4a shows the impedance spectra for the $Ce(NO_3)_3.6H_2O$ modified sol-gel coating before and after the defect formation as a function of the immersion time. The impedance value at low frequencies (LF) for the sample without the defect is close to 1.9 MΩ cm^2 during the first hours of the immersion. After 3 days of immersion a small drop of the impedance value at LF is observed (1.6 MΩ cm^2), that can be associated with the water uptake through the pores and/or defects in the coating [15]. For a longer immersion time (3 to 7 days), the impedance value at LF increases rapidly and maintains high values.

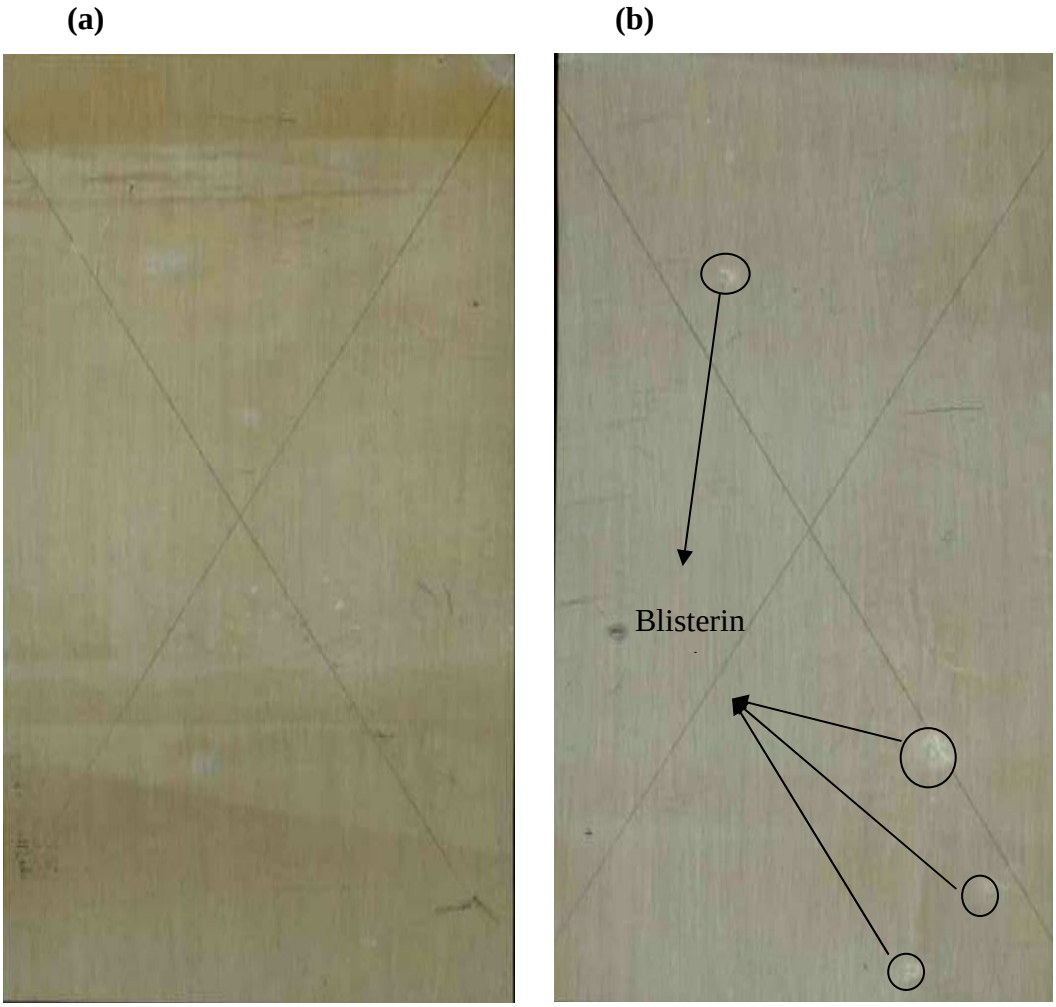

Figure 3. Photographs of the 304L stainless steel surfaces coated with the sol-gel coatings modified with $Ce(NO_3)_3.6H_2O$ (a) and CeO_2 nanoparticles (b) after 2000 hours of salt spray exposure.

After 7 days of immersion, a defect was induced on the coating surface in order to create a corroding area. 1 hour after application of this defect, the impedance value at LF reveals a marked decrease, which is close to 0.119 MΩ cm^2, as expected, since the coating is damaged. However, 1 day after the defect application the impedance value at LF shows a pronounced increase (1.6 MΩ cm^2). With further increase of the immersion time, a small drop of the LF impedance values is observed. This increase of impedance value can be attributed to the self-healing effect of $Ce(NO_3)_3.6H_2O$ on the corrosion spots [27]. This effect can originate from the release of the cerium near the coating defects. Subsequently, cerium produces insoluble hydroxides by its reaction with hydroxyl groups from cathodic reactions [22]. These hydroxides, together with corrosion products, decrease the cathodic current and consequently reduce the overall corrosion rate.

The shape of the phase angle plot in Figure 4b indicates the presence of two time constants before and after the application of the defect, which can be attributed to the response of the silane film (high frequency process) and to the response of processes occurring at the silane film/substrate interface (low frequency time constant).

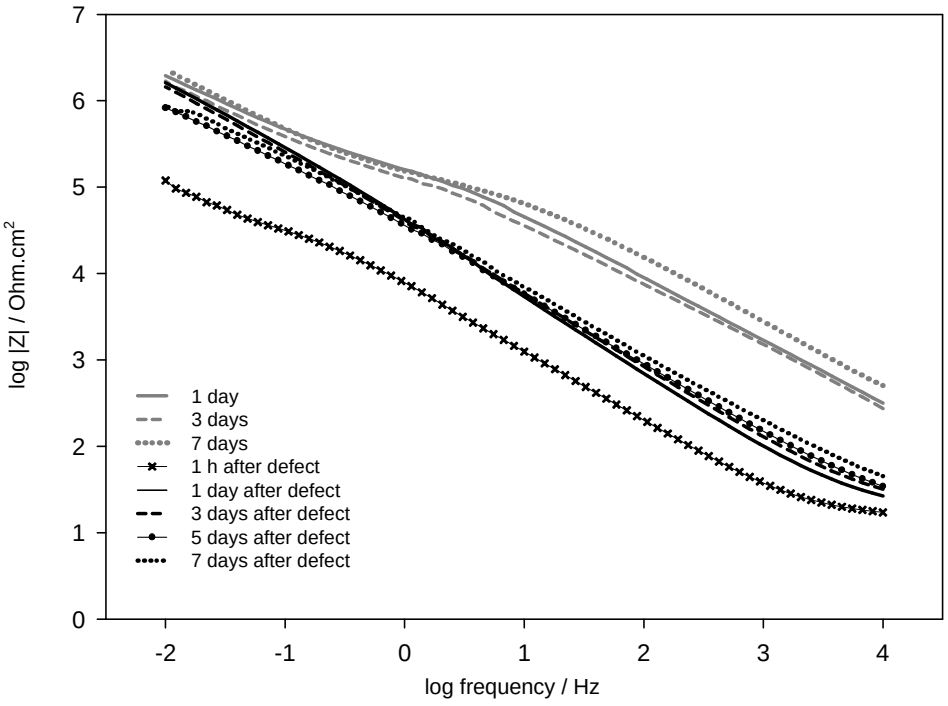

A

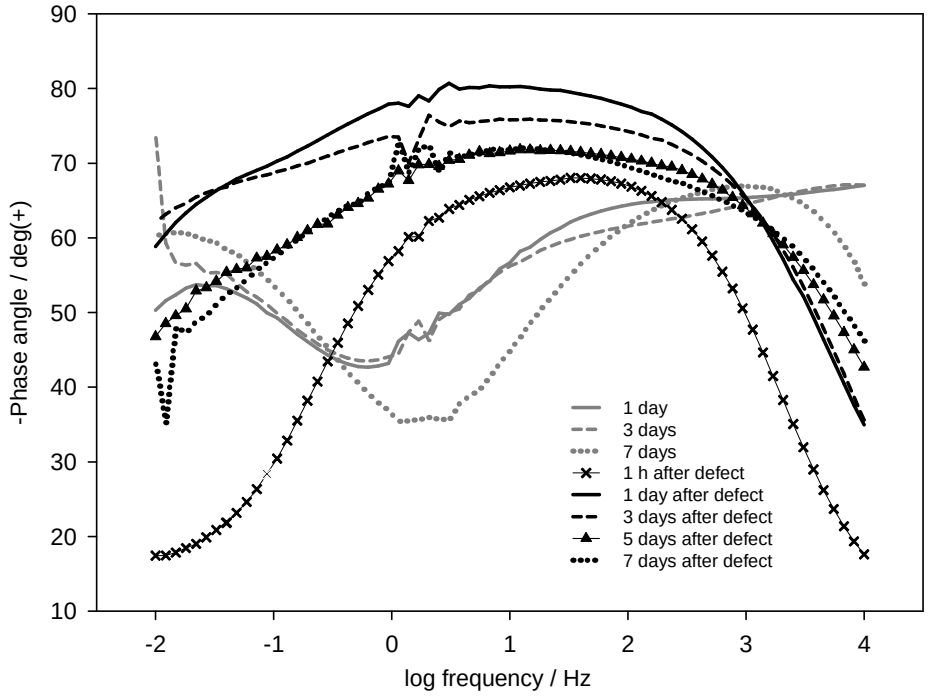

B

Figure 4. EIS Bode modulus (a) and phase angle (b) plots obtained on the 304L stainless steel sample pre-treated with the silane film modified with cerium nitrate. Spectra were obtained during immersion in a 3.5% NaCl solution, before and after the application of the defect.

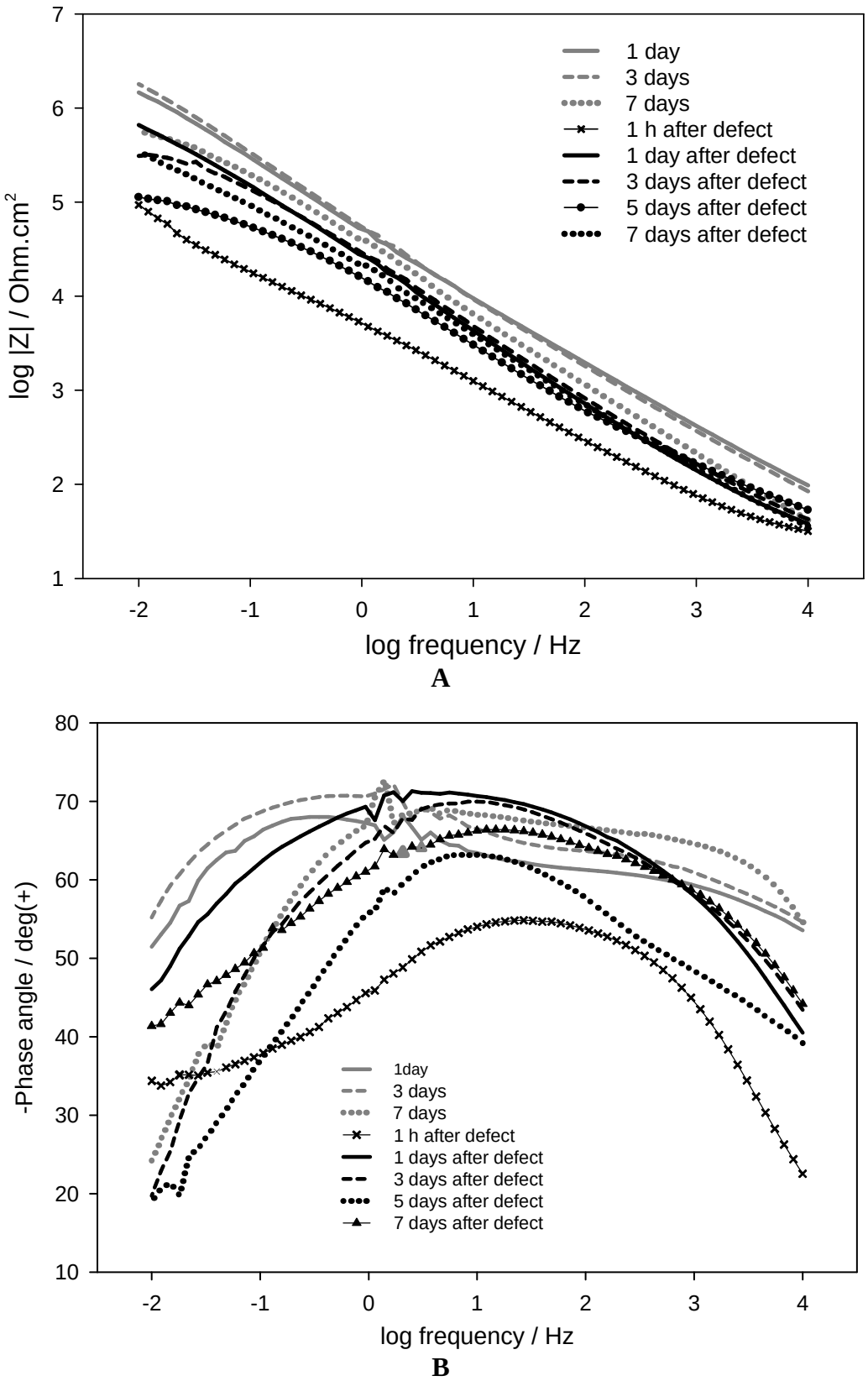

Figure 5. EIS Bode modulus (a) and phase angle (b) plots obtained on the 304L stainless steel sample pre-treated with the silane film containing CeO_2 nanoparticles. Spectra were obtained during immersion in 3.5% NaCl solution, before and after defect application.

For the coating modified with CeO_2 nanoparticles, a different trend is observed. Here, the total impedance of the system is lower than that for the $Ce(NO_3)_3.6H_2O$ modified sol-gel film. In addition the impedance values decrease rapidly with time before and 5 days after the application of the defect (Figure 5a). 7 days after the defect application, the impedance values increase, suggesting that the coating was still providing some protection.

Before the application of the defect and during the initial stage of immersion, the EIS spectra present two time constants (Figure 5b). With the increase of the immersion time, the one at high frequencies remains obvious but the other one at low frequencies becomes less defined. After the application of the defect, the phase angle plot indicates the presence of one time constant at high frequencies, which can be ascribed to corrosion process on the substrate, although no coating degradation was observed for the sol-gel coating containing CeO_2 nanoparticles.

A more detailed interpretation of the EIS measurements was performed by fitting the experimental plots using equivalent electrical circuits (EECs). Constant phase elements (CPE) instead of capacitances were used for all fittings presented in the work. Such modification is obligatory when the phase angle of capacitor is different from −90º. The impedance of the CPE depends on frequency according to the following equation [28]:

$$\frac{1}{Z} = Q\left(j\omega\right)^n \tag{1}$$

where Z is the impedance, Q a parameter numerically equal to the admittance (1/|Z|) at $\omega = 1$ rad s^{-1}, ω the frequency, and $n \leq 1$ a power coefficient calculated as ratio of phase angle at maximum of corresponding time constant to −90º. The capacitance values for the different elements in the equivalent circuit were calculated using the following equation [28]:

$$C = Q\omega_{\max}^{n-1} \tag{2}$$

where ω_{max} is the frequency at which the imaginary impedance reaches a maximum for the respective time constant.

The equivalent circuits used were chosen based on the number of time constants and analysis of the quality of the fits [29]. For the sol-gel coatings doped with cerium nitrate, the equivalent circuit can be described as shown in Figure 6a. It consists of the following elements: the electrolyte resistance, R_s, the non-ideal capacitance of the coating, CPE_c, the resistance presented by the pores or defects to the passage of the electrolyte, R_{po}, the non-ideal capacitance of the double layer between the metal surface and the electrolyte which is soaking the corrosion products nearby the pore, CPE_d, the charge transfer resistance of the metal, R_t, and the Warburg finite impedance, W. The Warburg impedance and the constant phase element (CPE) with a n value around 0.5 (the last known as “infinite diffusion”) are used to model the increasing ionic conductivity due to the corrosion process occurring inside the pores [15].

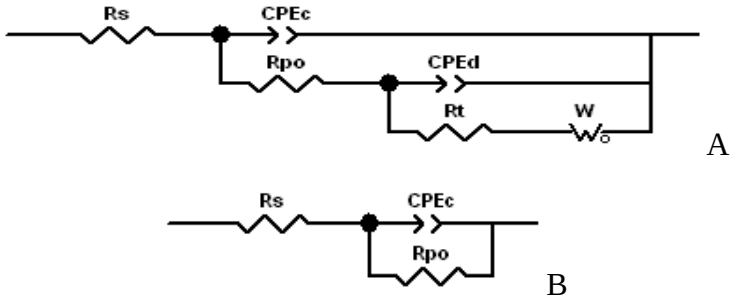

Figure 6. The equivalent circuits used for numerical fitting of the EIS data during immersion in 3.5% NaCl solution. (a) cerium nitrate modified sol-gel coating before and after defect application, sol-gel film containing CeO_2 nanoparticles before defect application; (b) sol-gel film containing CeO_2 nanoparticles after defect application.

For the sol-gel coatings containing the CeO_2 nanoparticles, the impedance results were fitted using two different equivalent circuits. Before the application of the defect, the EIS spectra were simulated with an equivalent circuit consisting of two time constants (Figure 6a), and after the application of the defect the spectra were simulated with equivalent circuit consisting of one time constant (figure 6b).

Figures 7 and 8 depict the evolution of the fitting parameters used for the numerical simulation of the experimental results. For the sol-gel coatings doped with cerium nitrate (Figure 7), before the application of the defect, the high frequency resistance values show a slight decrease during the first hours of immersion due to the development of conductive pathways inside the silane film [12]. The resistance remains nearly constant, around 0.132 MΩ cm^2 during the seven days of immersion. The CPE values at high frequency are around 0.95 µFcm^{-2} and show a slight decrease with time. The low frequency behavior, on the other hand, is characterized by a resistance value that increases from 8.404 MΩ cm^2 during the first hours of immersion up to 174 MΩ cm^2 after seven days of immersion. Its CPE values are around 2.7 µFcm^{-2} and remain nearly constant during the seven days of immersion.

1 day after the application of the defect there is an increase in the high frequency resistance (1.47 MΩ cm^2), but the values decrease slightly up to the end of experiment. The CPE values are around 4.7 µFcm^{-2} and increase with time. In contrast to the drop of the high frequency resistance, the low frequency resistance shows an increase from 1.2 MΩ cm^2 one day after defect application up to 11 MΩ cm^2 seven days after defect application. The CPE values decrease from 3.6 µFcm^{-2} down to 3.19 µFcm^{-2}. The evolution of the fitting parameters shows that the silane coating partially recovers its protective properties. Since the low frequency behavior can be assigned to the corrosion process occurring at the interface, it is possible to conclude that this process was slowed down.

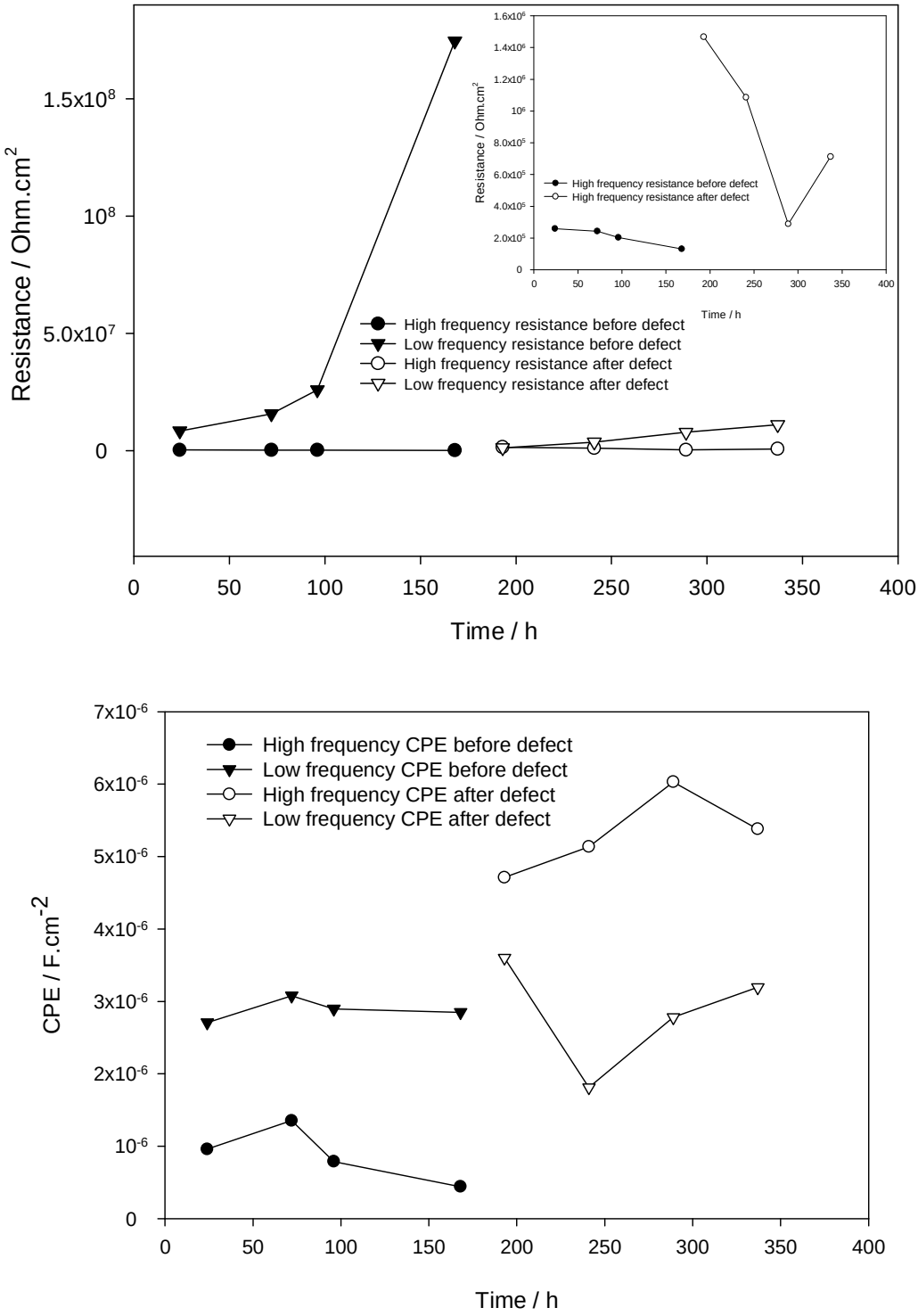

Figure 7. Evolution of the fitting parameters for the sol-gel coating modified with cerium nitrate.

For the sol-gel coatings containing CeO_2 nanoparticles (Figure 8), before the application of the defect, a small increase of the resistance value after 7 days of immersion can be observed, which can be ascribed to the blocking of the cerium oxide or hydroxide in the pores or defects [12, 28]. The CPE values are around 6.74 μFcm^{-2} and remain nearly constant during the seven days of immersion. At low frequencies, the resistance values increase with time, indicating that cerium oxide/hydroxide was

formed with the release of CeO_2 from the sol-gel matrix [12, 26]. After seven days of immersion, the resistance decreases to 2.95 MΩ cm^2, suggesting the occurrence of pitting corrosion on the substrate. Correspondingly, the CPE values increase rapidly with immersion time due to the breakage of the oxide/ hydroxide layer in this stage [12, 26].

After the application of the defect the resistance values decrease slightly with immersion time up to the end of experiment, indicating the degradation of this coating. Accordingly, the CPE values show a drop after 3 days of immersion 8.68 μFcm^{-2} and pass through a maximum and then decrease again (13.15 μFcm^{-2}), due to saturation of electrolyte in the sol-gel film.

The electrochemical tests show that the modification of the silane sol-gel coating with cerium ions results in the formation of a protective coating, either in terms of barrier properties or self-inhibiting corrosion activity. The improved barrier properties can be correlated with a higher degree of reactive silanol groups —$Si(OH)_3$ and more condensed species that may contribute to increase the silane solution viscosity and coating thickness [30].

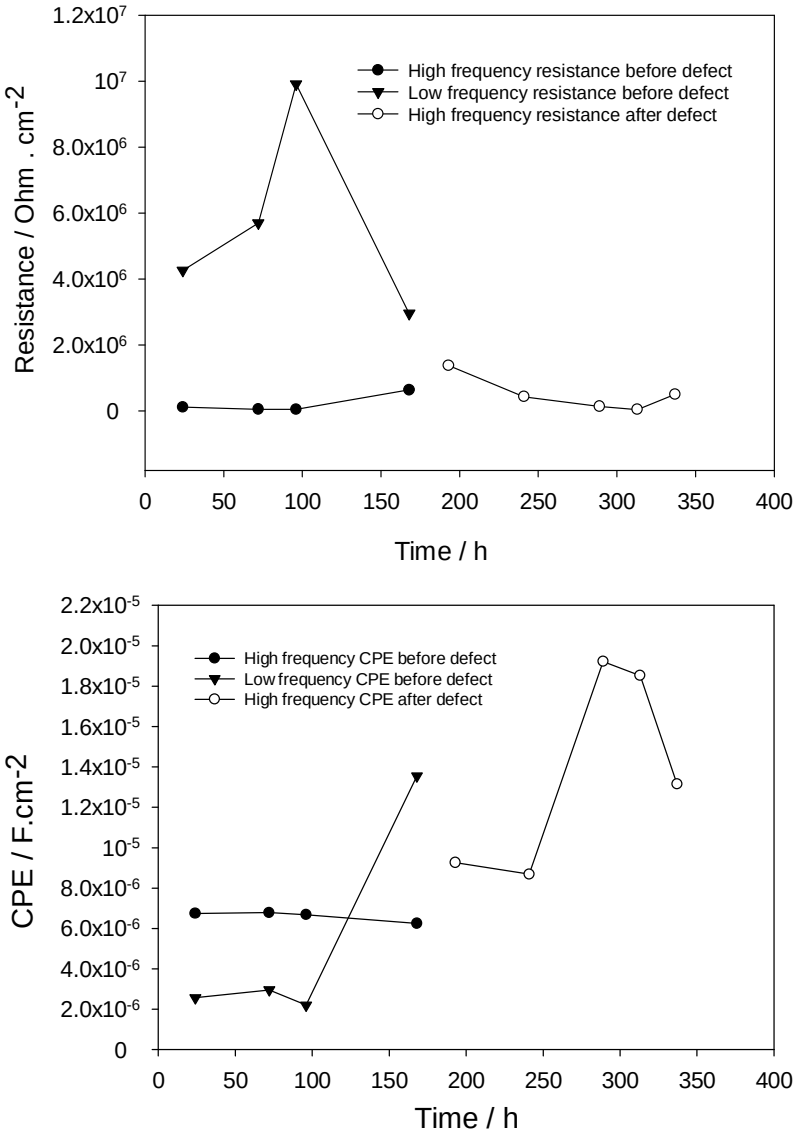

Figure 8. Evolution of the fitting parameters for the sol-gel coating containing CeO_2 nanoparticles.

3.5. Potentiondynamic polarization results

In order to assess more information on the mechanisms associated with the electrochemical behavior of these systems, potentiodynamic polarization measurements were performed. The potentiodynamic polarization curves obtained on the scratched samples after 1 hour of immersion are depicted in Figure 9. Table 1 summarizes the electrochemical parameters obtained from these measurements.

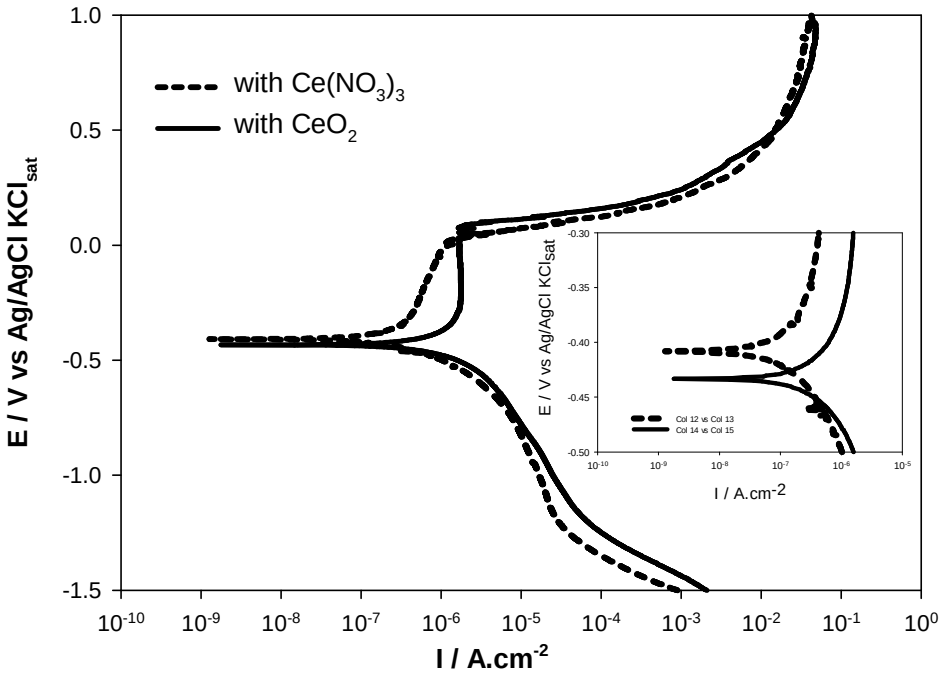

Figure 9. Potentiodynamic polarization curves of the sol-gel coating modified with cerium nitrate and sol-gel coating containing CeO_2 nanoparticles obtained after 1 hour immersion in a 3.5 % NaCl solution. For comparative purposes a plot is also inserted, in which the potential is depicted as the difference between the imposed potential and the corrosion potential. This approach allows a better separation of the anodic and cathodic polarization effects.

Table 1. Summary of the electrochemical parameters obtained from the polarization measured in a 3.5% Nacl solution.

sample	E_{corr} (V)	I_{corr} (A cm^{-2})	b_c (V/dec)	b_a (V/dec)	Passive area (V)
With $Ce(NO_3)_3$	-0.408	1.361×10^{-7}	0.187	0.950	-0.340 to 0.013
With CeO_2	-0.434	4.993×10^{-7}	0.230	0.116	-0.403 to 0.092

In comparison to the sol-gel coating containing CeO_2 nanoparticles, the $Ce(NO_3)_3$ doped sol-gel coating shows a lower corrosion current density, i_{corr}, around 0.316 µA.cm^{-2}. In addition its potential is shifted to a higher value (-0.408 V). This coated sample shows a passivation range of

approximately -340 mV to 13 mV over its corrosion potential. This behavior was improved by the protective barrier characteristic of the coating, as reported before [22].

As a comparative result, the sol-gel coating containing CeO_2 nanoparticles, presents a continuous potential range characterized by a control mechanism of equilibrium in the oxidation and reduction reactions. Also a wide passive plateau in the range of -403 mV to 92 mV above the corrosion potential was observed.

The d.c. polarization results show that the presence of cerium compounds shifts the corrosion potential towards nobler values, and decreases the anodic currents and changes the kinetics of the anodic processes, as reported before [22]. These effects are much more marked for the $Ce(NO_3)_3$ modified sol-gel coatings when compared to the sol-gel coatings containing CeO_2 nanoparticles.

4. CONCLUSIONS

Pre-treatments based on the use of organofunctional silane solutions modified with a corrosion inhibitor can benefit from additional active corrosion protection when an appropriate inhibitor is used. Cerium nitrate and cerium oxide are demonstrated here as possible additives which can provide a self-healing ability in combination with their good barrier properties of the sol-gel films.

Microscopic observations confirm the formation of transparent cerium modified sol-gel films without any defects and cracks. The results reveal the formation of a comparatively smooth nanostructure surface with a small heterogeneity in coating thickness in the sol-gel coatings modified with $Ce(NO_3)_3.6H_2O$. Also these results confirm the integral maintaining the surface morphology of the sol-gel coatings modified with CeO_2 nanoparticles, after short time corrosion tests (14 days immersion in 3.5% NaCl solution).

Corrosion tests results indicate that the CeO_2 nanoparticles have good corrosion inhibition properties on scratched surfaces due to ability to complex other species, therefore contributing for the stabilization of the passive film. In this way, these particles have an anodic inhibition mechanism.

The positive impact, in the barrier properties, corrosion inhibition and self –repair of defects, is significantly improved with modification of the silane solution with cerium nitrate solution. The cerium ions have the ability to change the silane solution chemistry, promoting the formation of reactive silanol group and also of more condensed species. The cerium nitrate provides the best corrosion protection either in intact sol-gel films or in the presence of scratches.

ACKNOWLEDGEMENTS
The authors wish to acknowledge Ghent University for financial support of this study. The authors would also like to thank Michel Moors and Sandra Van Vlierberghe for their technical assistance.

References

1. R.L. Twite, G.P. Bierwagen, *Prog. Org. Coat*. 33 (1998) 91.
2. A. Franquet, C. Le Pen, H. Terryn, J. Vereecken, *Electrochim. Acta*. 48 (2003) 1245.
3. D. Zhu, W.J. van Ooij, *Corros. Sci.* 45 (2003) 2177.

4. A.M. Beccaria, L. Chiaruttini, *Corros. Sci.* 41 (1999) 885.
5. A. Beccaria, G. Padeletti, G. Montesperlli, L. Chiaruttini, *Surf. Coat. Technol*. 111 (1999) 240.
6. D.Q. Zhu, W.J. van Ooij, *Electrochim. Acta*. 49 (2004) 1113.
7. D.Q. Zhu, W.J. van Ooij, *Prog. Org. Coat*. 49 (2004) 42.
8. A. Cabral, R.G. Duarte, M.F. Montemor, M.L. Zheludkevich, M.G.S. Ferreira, *Corros. Sci*. 47 (2005) 869.
9. V. Palanivel, D. Zhu, W.J. van Ooij, *Prog. Org. Coat*. 47 (2003) 384.
10. F. Deflorian, S. Rossi, M. Fedel, C. Motte, *Prog. Org. Coat*. 69 (2010) 158.
11. A.M. Cabral, W. Trabelsi, R. Serra, M.F. Montemor, M.L. Zheludkevich, M.G.S. Ferreira**,** *Corros. Sci.* 48 (2006) 3740.
12. M.F. Montemor, M.G.S. Ferreira, *Electrochim. Acta.* 52 (2007) 6976.
13. H. Wang, R. Akid, *Corros. Sci*. 50 (2008) 1142.
14. W. Trabelsi, P. Cecilio, M.G.S. Ferreira, M.F. Montemor, *Prog. Org. Coat*. 54 (2005) 276.
15. A. Pepe, M. Aparicio, A. Durán, S. Ceré, *J. Sol-Gel Sci. Techn*. 39 (2006) 131.
16. A. Pepe, M. Aparicio, S. Ceré, A. Durán, *J. Non-Cryst. Solids*. 348 (2004) 162.
17. W. Trabelsi, E. Triki, L. Dhouibi, M.G.S. Ferreira, M.L. Zheludkevich, M.F. Montemor, *Surf. Coat. Technol.* 200 (2006) 4240.
18. N.N. Voevodin, N.T. Grebasch, W.S. Soto, F.E. Arnold, M.S. Donley, *Surf. Coat. Technol*. 140 (2001) 24.
19. N.C.R. Navarro, S. A. Pellice, A. Durán, S. Ceré, M. Aparicio, *J. Sol-Gel. Sci. Technol*. 52 (2009) 31.
20. M. Schem, T. Schmidt, J. Gerwann, M. Wittmar, M. Veith, G.E. Thompson, I.S. Molchan, T. Hashimoto, P. Skeldon, A.R. Phani, S. Santucci, M.L. Zheludkevich, *Corros. Sci.* 51 (2009) 2304.
21. M.F. Montemor, R. Pinto, M.G.S. Ferreira, *Electrochim. Acta* 54 (2009) 5179.
22. R. Zandi Zand, K. Verbeken, A. Adriaens, *Prog. Org. Coat.* (2012) http://dx.doi.org/10.1016/j.porgcoat.2012.06.008.
23. R. Zandi Zand, Investigation of corrosion, abrasion and weathering resistance in hybrid nanocomposite coatings based on epoxy-silica, Thesis, Azad University-Tehran North Branch, (2005).
24. R. Zandi Zand, K. Verbeken, A. Adriaens, *Prog. Org. Coat*. 72 (2011) 709.
25. ASTM B117 - 11 Standard Practice for Operating Salt Spray (Fog) Apparatus, G01.05, Book of Standards Volume: 03.02 (2011).
26. ASTM Standards for Corrosion Testing of Metals: 3rd Edition, ASTM International, W. Conshohocken, PA, 2008.
27. M.L. Zheludkevich, K.A. Yasakau, A.C. Bastos, O.V. Karavai, M.G.S. Ferreira, *Electrochem Commun.* 9 (2007) 2622.
28. H. Shi, F. Liu, E. Han, *Mater Chem Phys*. 124 (2010) 291.
29. M.L. Zheludkevich, R. Serra, M.F. Montemor, K.A. Yasakau, I.M. Miranda Salvado, M.G.S. Ferreira, *Electrochim Acta*. 51 (2005) 208.
30. M.F. Montemor, M.G.S. Ferreira, *Prog. Org. Coat*. 63 (2008) 330.